Capillarity

Vol. 18, No. 3, p. 106-116, 2026

Original article

Pore-scale numerical study on CO_2 flooding brine in homogeneous and fractured porous media: Implication to the geological storage of greenhouse gas in saline aquifers

Chi Liu, Zongjin Li, Zeguang Dong, Yingge Li, Dongxing Du*

Geo-Energy Research Institute, College of Electromechanical Engineering, Qingdao University of Science and Technology, Qingdao 266100, P. R. China

Keywords:
Pore scale
numerical study
CO_2 displacing brine
homogeneous porous media
fractured porous media

Cited as:
Liu, C., Li, Z., Dong, Z., Li, Y., Du, D. Pore-scale numerical study on CO_2 flooding brine in homogeneous and fractured porous media: Implication to the geological storage of greenhouse gas in saline aquifers. Capillarity, 2026, 18(3): 106-116.
https://doi.org/10.46690/capi.2026.03.03

Abstract:
CO_2 injection into deep saline aquifer reservoirs is promising for long-term storage of greenhouse gases. To reveal the pore-scale mechanisms underlying CO_2-brine displacement in subsurface formations, computational fluid dynamics simulations were performed in digitally reconstructed homogeneous and fractured porous media. Results showed that the displacement processes in the two types of porous media were governed by fundamentally different mechanisms. In homogeneous media, capillary forces associated with complex pore-throat geometries dominated the displacement behavior. Under low driving forces, the migration of CO_2 was strongly restricted by capillary trapping, resulting in limited removal of brine. As the driving force increased, the injection of CO_2 could overcome local pore-throat resistance and achieve effective displacement of brine. In fractured porous media, fracture structures provided preferential flow paths with lower hydraulic resistance, allowing the breakthrough of CO_2 to occur under relatively low driving forces. However, after the breakthrough, fractures contributed only marginally to additional displacement of brine from the rock matrix, as CO_2 preferentially flowed through the fracture channels. The present work provides quantitative and mechanistic insights into CO_2-brine displacement processes in porous media, offering valuable guidance for the assessment and optimization of geological carbon storage strategies.

1. Introduction

Injecting CO_2 into geological formations enables safe and long-term storage of greenhouse gases (Du et al., 2018; Li et al., 2022; Kumari et al., 2024; Peng et al., 2025). Consequently, studies focusing on the characterization and displacement behaviors of CO_2-involved multiphase flow in porous media have attracted increasing attention in recent years (Seyyedi et al., 2020; Liu et al., 2022b; Song et al., 2022; Wang et al., 2023; Liu et al., 2025).

For geological storage through CO_2 injection into deep saline aquifers, existing studies can be broadly categorized into experimental and simulation works. Experimental studies enable successful identification of key controlling factors in multiphase displacement processes, including wettability (Saeedi et al., 2011; Hu et al., 2017; Shao et al., 2025), interfacial tension (IFT) (Krevor et al., 2012; Cao et al., 2016), injection strategies (Zhang et al., 2017; Adebayo, 2018; Patmonoaji et al., 2019; Ding et al., 2024; Zhao et al., 2025). However, due to their macroscale nature, experimental approaches are often insufficient to provide detailed mechanistic

Yandy Scientific Press

*Corresponding author.
E-mail address: 15242964233@163.com (C. Liu); lizongjin0914@163.com (Z. Li); dong200112@163.com (Z. Dong); liyingge@qust.edu.cn (Y. Li); du-dongxing@qust.edu.cn (D. Du).

Received December 20, 2025; revised January 21, 2026; accepted February 12, 2026; available online February 15, 2026.

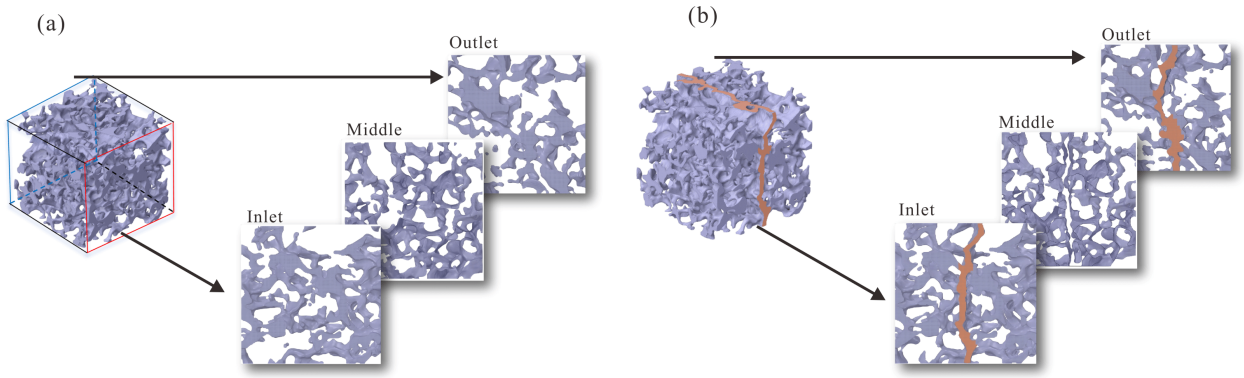

Fig. 1. The digital models of the (a) homogeneous and (b) fractured porous media.

understanding of complex multiphase flows at pore-scale. To overcome these limitations, pore-scale numerical approaches have been increasingly adopted. Among them, digital rock physics (DRP) has demonstrated strong capability in revealing pore-scale transport mechanisms due to its ability to accurately reconstruct complex internal pore geometries (Blunt et al., 2013; Han et al., 2020; Song et al., 2025; Yang et al., 2025; Du et al., 2026). By applying multiphase flow simulations to reconstructed porous media, a growing number of studies have been performed on CO_2 displacing brine and/or water processes. The numerical methods employed include the lattice Boltzmann method (Li et al., 2024a; Ren et al., 2025; Aslannezhad et al., 2025; Ryou et al., 2025), pore network model, and computational fluid dynamics (CFD) (Yang et al., 2023). While the computational domains range from two-dimensional to three-dimensional porous media. Notably, most existing DRP studies have focused on homogeneous porous media. In practical geological formations, heterogeneity is ubiquitous and can significantly influence the multiphase displacement behavior (Du et al., 2017; Muñoz-Ibáñez et al., 2020; Xiao et al., 2022; Diao et al., 2024; Wang et al., 2026). Despite its importance, the specific role of fracture-induced heterogeneity in CO_2-brine displacement processes remains insufficiently examined.

In the present paper, pore-scale numerical simulations are carried out on CO_2 displacing brine processes using the DRP technique. Both homogeneous and heterogeneous porous media are considered. The homogeneous porous media were constructed from high-resolution micro-CT images. The heterogeneous porous media model is created by introducing fracture structures into the homogeneous porous media. A sophisticated CFD approach is employed to study the effect of formation's heterogeneity on the displacement characteristics of brine by CO_2. Parametric studies are also performed to examine the influences of IFT and wettability on the displacement process. The control mechanisms of the fractured structure are revealed based on two-phase fluid distribution, gas breakthrough pressure, and ultimate displacement efficiency. The work provides insights into CO_2-brine displacement behavior in rock formations to support the carbon capture, utilization, and storage industry.

2. Numerical details

2.1 Digital rock models and the CFD algorithms

A digital rock model was constructed to serve as a representative elementary volume (REV). This model was used to explore the pore-scale characteristics and multiphase displacement behaviors. The REV of the homogeneous model, shown in Fig. 1(a), was reconstructed from micro-CT images of a Bentheimer core with 23% porosity (Ramstad, 2018). The REV consisted of $200 \times 200 \times 200$ pixels at image pixel resolution of 7 μm. Previous studies have shown that a REV of this size performs satisfactorily in two-phase displacement simulations. This applies specifically to homogeneous porous media (Najafi et al., 2023; Wang et al., 2025). For the heterogeneous model, shown in Fig. 1(b), a fracture network was introduced into the homogeneous REV. The network had an average aperture of 49.9 μm and was used to mimic the fracture structures. Detailed procedures for reconstructing and screening the homogeneous core REV can be found in a previous work (Liu et al., 2022a). Procedures for reconstructing the fractured porous media model are described in previous studies (Li et al., 2024b; Dong et al., 2025).

The steady-state displacement of brine by a gas is numerically studied using the mixture model (Zeidan et al., 2019; Tronci et al., 2021). The study was based on the assumptions of laminar flow, constant system properties, and no sliding velocity between the two-phase fluids. The mixture's mass and momentum conservation equations are listed in Eqs. (1)-(2) (Wan et al., 2022), incorporating multiple interaction forces, including IFT and wettability effects.

The mass conservation is given by:

$$\nabla \cdot (\rho_m \mathbf{u}_m) = 0 \tag{1}$$

The momentum conservation is given:

$$\begin{aligned} &\nabla \cdot (\rho_m \mathbf{u}_m \mathbf{u}_m) = \\ &-\nabla p + \nabla \cdot \left[\mu_m \left(\nabla \mathbf{u}_m + \nabla \mathbf{u}_m^{\mathrm{T}}\right)\right] + \rho_m \mathbf{g} + \mathbf{S}_m \end{aligned} \tag{2}$$

where p is pressure, $\mathbf{g}$ is the gravitational acceleration vector, and $\mathbf{S}_m$ accounts for capillary-related forces such as IFT and wettability. The mixture's density (ρ_m), viscosity (μ_m), and velocity vector ($\mathbf{u}_m$) are given by Eqs. (3)-(5), respectively.

Table 1. Basic physical properties of the multiphase fluid system.

Fluid type	Density (kg/m^3)	Viscosity (10^{-4} Pa·s)	IFT (N/m)	Water receding contact angle (°)
CO_2	654.45	0.526	0.029	14
Brine	1,054.2	5.85	0.029	14

Table 2. The simulation scenarios in the study.

Cases	Porous media	Inlet pressure (Pa)
1	Homogeneous	500
2		1,000
3		2,000
4		3,000
5	Fractured	500
6		1,000
7		2,000

$$\rho_m = \sum_{k=1}^{N} \alpha_k \rho_k \tag{3}$$

$$\mu_m = \sum_{k=1}^{N} \alpha_k \mu_k \tag{4}$$

$$\mathbf{u}_m = \frac{\sum_{k=1}^{N} \alpha_k \rho_k \mathbf{u}_k}{\rho_m} \tag{5}$$

where N is the phase number, and α_k, ρ_k, μ_k, and $\mathbf{u}_k$ denote the volume fraction, density, viscosity, and velocity vector of phase k, respectively.

To close the governing equations, the continuity equations for mass of each phase and the volume fraction constraint, as depicted in Eqs. (6) and (7), respectively, are used.

$$\nabla \cdot (\alpha_k \rho_k \mathbf{u}_k) = 0 \tag{6}$$

$$\sum_{k=1}^{N} \alpha_k = 1 \tag{7}$$

Eqs. (1)-(7) were solved numerically using ANSYS Fluent software. The least-squares cell-based method was adopted for evaluating the gradient. The PRESTO! scheme was used for discretizing the pressure term. The momentum conservation equations were discretized with the second-order upwind scheme. The mass conservation equations for different phases were discretized with the first-order upwind scheme (ANSYS Inc., 2022). These numerical configurations have been well justified in previous studies in complex porous media (Wan et al., 2022; Li et al., 2024b).

2.2 Simulation scenarios

Constant pressure condition was applied at both the inlet and outlet of the porous domain. By varying the inlet pressure, the CO_2-brine displacement characteristics were examined in terms of internal distribution of phases and the efficiency of brine's displacement by CO_2. The physical properties of CO_2 and brine, under a typical reservoir temperature of 70 °C and pressure of 20 MPa, are listed in Table 1. The density and viscosity data were retrieved from the material property platform (AP1700, 2025). The IFT and water receding contact angle were obtained from a previous work (Saraji et al., 2014).

All simulation scenarios are listed in Table 2. In homogeneous porous media, four simulation cases (Cases 1-4) were considered. Inlet pressures of 500, 1,000, 2,000, and 3,000 Pa were sequentially applied with a constant outlet pressure of 0 Pa. In the fractured porous media, three simulation cases (Cases 5-7) were considered. Pressure drops (Δp) of 500, 1,000, and 2,000 Pa were applied sequentially to investigate the CO_2-brine displacement process. Notably, the pressure gradients adopted in the simulations were consistent with those reported in relevant experimental studies (Al-Zaidi et al., 2018; Chang et al., 2021).

2.3 Grid sensitivity studies

Proper grid resolution is essential for ensuring the reliability of numerical simulations, particularly in complex porous media. In the present study, a grid sensitivity analysis was conducted based on the overall CO_2-brine displacement efficiency (denoted as η_o), which is defined mathematically by:

$$\eta_o = \frac{V_g}{V_o} \tag{8}$$

where V_g represents the pore volume occupied by the gas phase after displacement, V_o denotes the total pore volume of the porous domain, regardless of whether the medium is homogeneous or fractured. To ensure grid independence, mesh sensitivity analyses were performed for both homogeneous and fractured porous media. Fig. 2(a) illustrates the variation of CO_2-brine displacement efficiency with grid resolution in homogeneous porous media under the Δp of 2,000 Pa. The total number of grid cells lied within the range of 0.74-4.30 million. Fig. 2(b) presents the corresponding results for fractured porous media, with grid numbers varying from 0.86-3.81 million.

The results in Fig. 2(a) showed, when the number of grids exceeded 2.06 million, the displacement efficiency in the homogeneous model became stable. Further mesh refinement led to negligible changes in the results. A similar variation trend was observed for the fractured model in Fig. 2(b), showing that grid independence was achieved when the number of grids exceeded 2.30 million. Based on these results, grid systems with 2.06 million and 2.30 million cells were adopted for the homogeneous and fractured models, respectively.

3. Results and discussion

In this section, a comparative analysis of the displacements of brine by CO_2 in homogeneous and fractured porous media is presented. The analysis was based on pore-scale two-phase distributions and displacement efficiency results. Parametric studies on key factors such as IFT and wettability were also performed. Finally, a comprehensive discussion of the simulation results is presented.

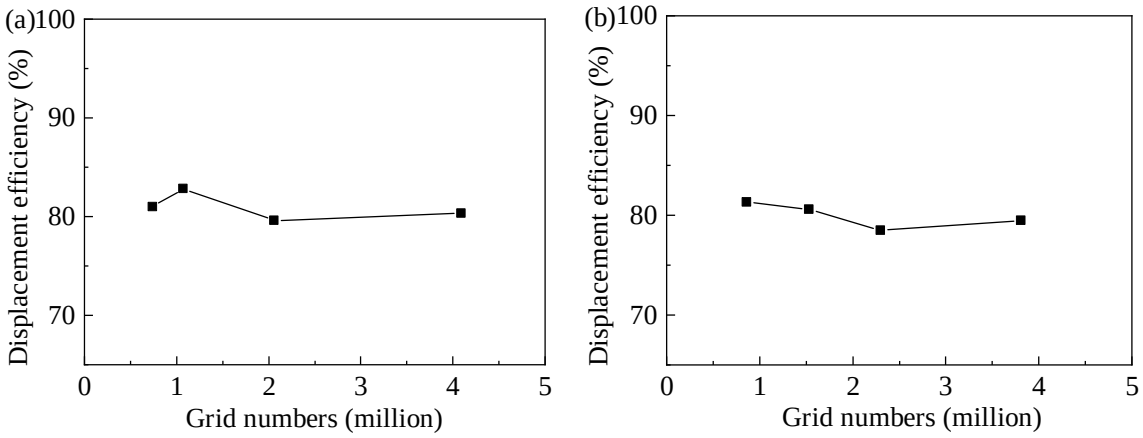

Fig. 2. Grid independent study based on the CO_2 displacing brine efficiency results ($\Delta p = 2{,}000$ Pa): (a) Homogeneous and the (b) fractured digital porous media.

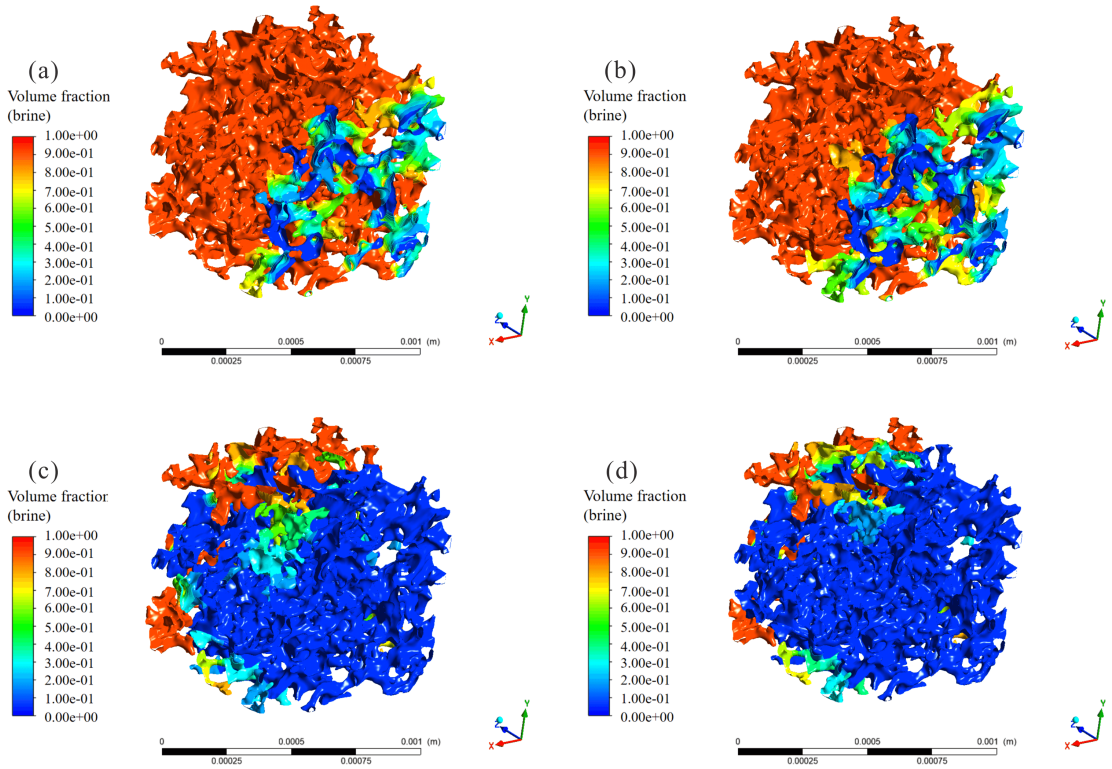

Fig. 3. Two phase fluid distributions after the CO_2 displacing brine processes (homogeneous porous media): (a) $\Delta p = 500$ Pa, (b) $\Delta p = 1{,}000$ Pa, (c) $\Delta p = 2{,}000$ Pa, and (d) $\Delta p = 3{,}000$ Pa.

3.1 Distribution of the two-phase fluid in homogeneous porous media

Corresponding to Cases 1-4 (see Table 2), the distributions of two-phase fluid after CO_2-brine displacement are shown in Figs. 3(a)-3(d) under sequential pressure drops of 500, 1,000, 2,000, and 3,000 Pa. The results showed that a critical pressure drop existed for achieving effective gas flooding in porous media. In Figs. 3(a) and 3(b), the injected CO_2 could not fully displace the brine-saturated medium at the Δp values of 500 Pa and 1,000 Pa. A large amount of brine (red) remained unflooded. When the pressure drop was increased to 2,000 Pa or higher, successful gas flooding was achieved as shown in Figs. 3(c) and 3(d). A sufficient amount of gas phase (blue) remained distributed within the homogeneous porous domain. Therefore, the critical pressure drop for the CO_2-brine displacement process lied within the range of 1,000-2,000 Pa.

To scrutinize the mechanisms behind the critical pressure drop, detailed analyses on the pore-scale distributions of phases were carried out. Figs. 4(a) and 4(b) show enlarged

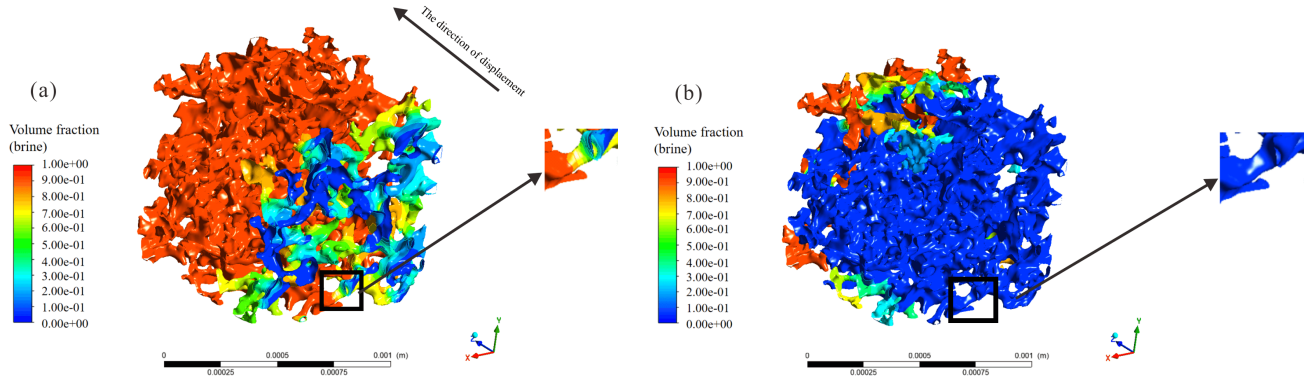

Fig. 4. Comparisons on two phase fluid distributions in a specific pore throat structure after CO_2 displacing brine: (a) $\Delta p = 1{,}000$ Pa and (b) $\Delta p = 2{,}000$ Pa.

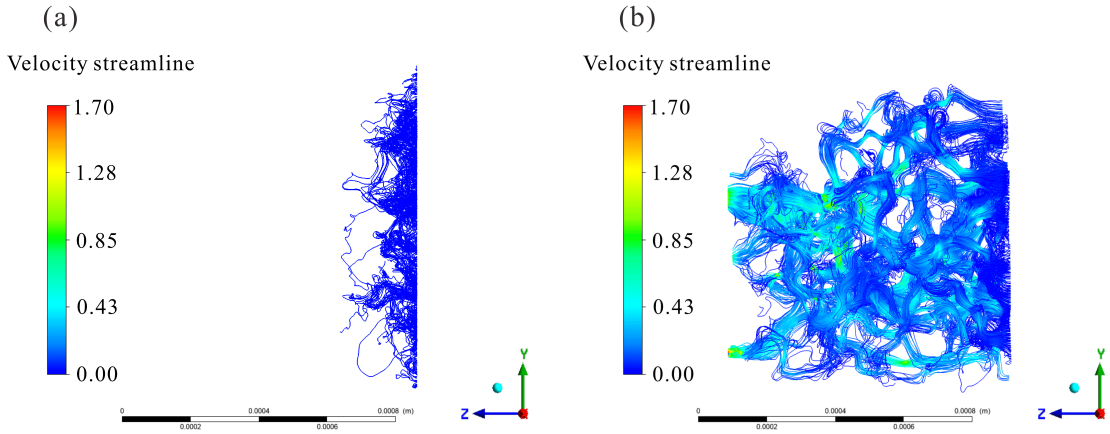

Fig. 5. The streamline distribution results after CO_2 displacing brine from homogeneous porous media: (a) $\Delta p = 1{,}000$ Pa and (b) $\Delta p = 2{,}000$ Pa.

views of the distributions of phases at a pore throat located near the inlet region. The results corresponded to pressure drops of 1,000 and 2,000 Pa. As shown in Fig. 4(a), the lower pressure drop of 1,000 Pa could not push the gas phase through the narrow pore throat due to strong capillary forces. When the pressure gradient was increased to 2,000 Pa in Fig. 4(b), the gas phase could pass through the pore throat. The increased pressure gradient overcame interfacial forces and released the capillary-trapped fluid. Further comparisons of the internal two-phase flooding processes in homogeneous porous media were illustrated using streamlines (flow streamline results). Figs. 5(a) and 5(b) display the distribution of streamlines under the pressure drops of 1,000 and 2,000 Pa, respectively. Fig. 5(a) shows the detailed blockage of the injected gas phase under a lower pressure drop of 1,000 Pa. Fig. 5(b) illustrates the gas breakthrough paths under a higher pressure drop of 2,000 Pa.

3.2 Distribution of two-phase fluid in fractured porous media

To further clarify the influence of fracture continuity on the behavior of two-phase flow in porous media, a series of numerical simulations was conducted. In these simulations, the aperture connectivity was systematically varied while other parameters were kept constant. More specifically, Cases 5-7 (see Table 2) were designed to represent fractured porous media with continuous aperture structures of different geometries. By comparing the two-phase displacement responses among these cases, the role of continuous fracture apertures can be quantitatively evaluated. Their influence on flow paths, distribution of phases, and displacement efficiency was analyzed.

After the CO_2-brine displacement in the fractured porous media under the pressure drops of 500, 1,000 and 2,000 Pa, the gas and brine saturation distributions are shown in Figs. 6(a)-6(c). At the lowest pressure gradient in Fig. 6(a), the injected CO_2 failed to flood the brine-saturated porous media. This occurred despite the presence of fractures. When the injection pressure was increased to 1,000 and 2,000 Pa in Figs. 6(b) and 6(c), the injected CO_2 successfully completed the displacement from the inlet to the outlet.

A detailed analysis was conducted to examine the internal phase distributions in fractured porous media under the pressure drop values of 500 and 1,000 Pa. Figs. 7(a) and 7(b) illustrate the corresponding phase distributions. In

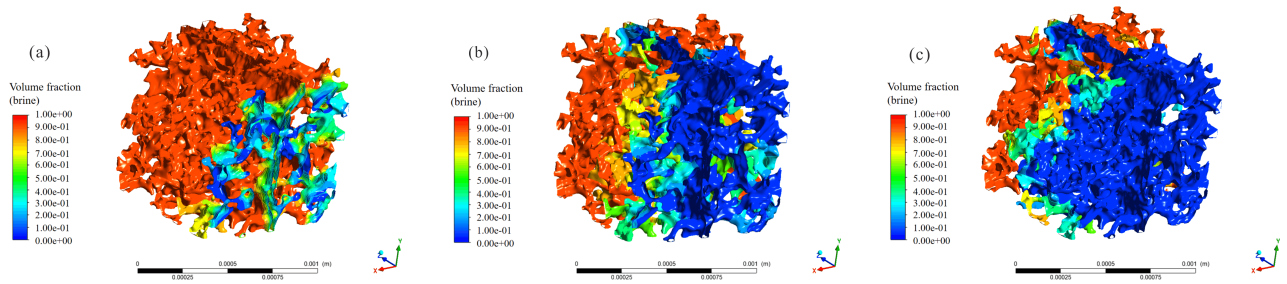

Fig. 6. Two phase saturation distribution results after CO_2 displacing brine (fractured porous media): (a) $\Delta p = 500$ Pa, (b) $\Delta p = 1{,}000$ Pa, and (c) $\Delta p = 2{,}000$ Pa.

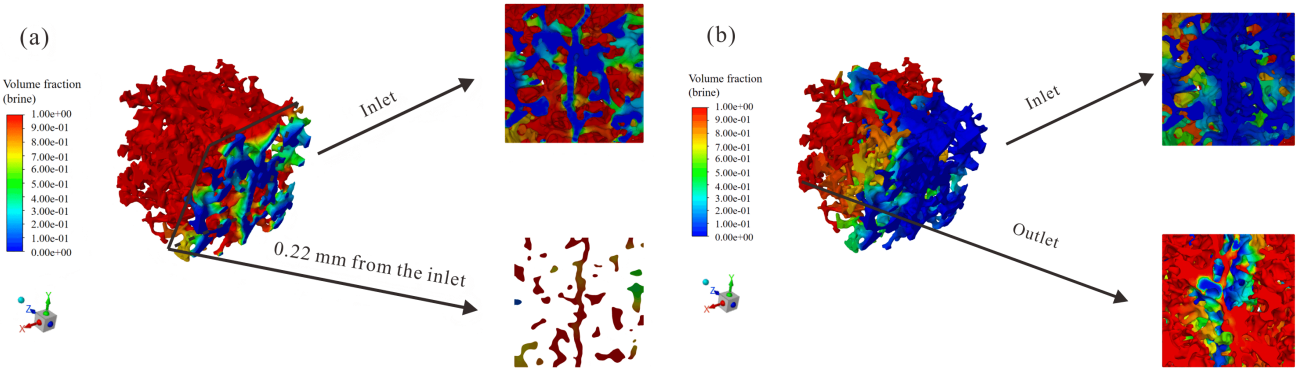

Fig. 7. Comparisons on phase distribution results in fractured porous media after CO_2 displacing brine: (a) $\Delta p = 500$ Pa and (b) $\Delta p = 1{,}000$ Pa.

Fig. 7(a), capillary blockade occurred during the CO_2-brine displacement process, even in the presence of fractures. More specifically, a distinct blockade region was observed approximately 0.22 mm from the core's inlet under the pressure drop of 500 Pa. When the pressure drop was increased to 1,000 Pa in Fig. 7(b), the injected CO_2 flushed the brine phase from the previously blocked region. It then achieved breakthrough along the fracture network towards the outlet. Comparing these results with those obtained for the homogeneous porous media (Figs. 3-5) clearly demonstrates that the presence of fractures substantially promotes the CO_2-brine displacement process. As shown in Figs. 6 and 7, gas breakthrough in fractured porous media occurred for the pressure drop values of 500-1,000 Pa, which were significantly lower than those (1,000-2,000 Pa) required in the homogeneous porous media.

The corresponding streamlines for the pressure drops of 500 and 1,000 Pa are shown in Figs. 8(a) and 8(b), respectively. These streamline patterns provided a clearer illustration of the displacement behavior of brine due to the injection of gas in fractured porous media. In Fig. 8(a), the gas injection paths were mainly concentrated within the fracture network. However, the injected gas did not achieve continuous breakthrough along any path, indicating strong blockade caused by IFT. Under a higher pressure drop of 1,000 Pa in Fig. 8(b), the injected gas successfully displaced brine through the fracture structure. This result demonstrated that the capillary force was effectively overcome, allowing gas breakthrough to occur.

3.3 Displacement efficiency in both types of porous media

In general, the gas-brine displacement efficiency is quantified by calculating the volumetric fraction of gas after the completion of gas injection process, as defined by Eq. (8). In fractured porous media, two distinct pore systems exist: The pore space within the base rock matrix and the fracture channel space. The displacement efficiency within the fracture network could approach 100% due to the continuous high-permeability paths in the fractures. Consequently, the displacement efficiency from the base matrix pores represented a more relevant metric for evaluating the geological storage potential of CO_2.

Therefore, a displacement efficiency for quantifying the recovery of brine solely from the base rock matrix (η_b) is introduced and defined by:

$$\eta_b = \frac{V_{g,bm}}{V_{bm}} = \frac{V_g - V_f}{V_o - V_f} \tag{9}$$

where V_g is the overall pore volume occupied by the gas phase after displacement, V_o denotes the total pore volume of the porous domain, either homogeneous or fractured, V_f is the pore volume of the fracture channels, excluding the base rock matrix, and the subscript *bm* refers to the base matrix, which represents the porous rock excluding fractures. Actually, Eq. (9) can be simplified to Eq. (8) for homogeneous media, where $V_f = 0$. This simplification is valid when the injected gas has flooded the fracture network and fully occupies the initially

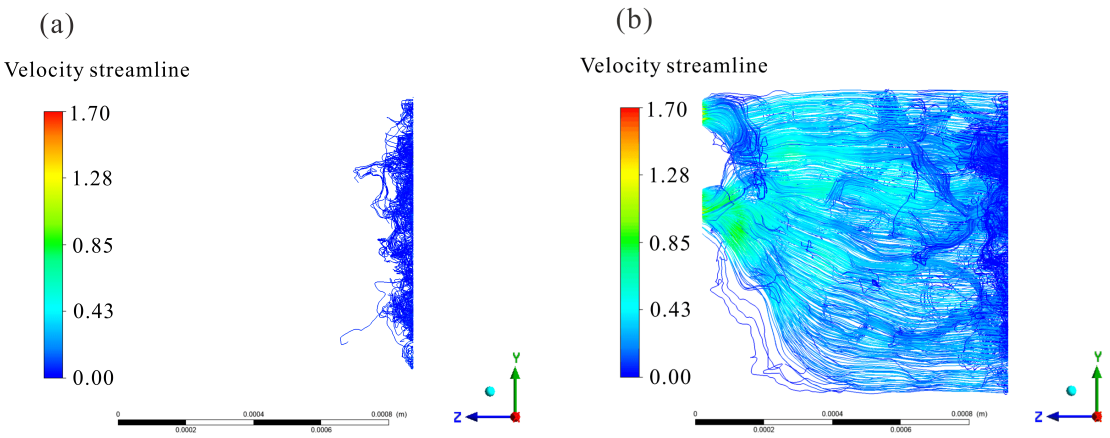

Fig. 8. The streamline distribution results after CO_2 displacing brine in fractured porous media: (a) $\Delta p = 500$ Pa and (b) $\Delta p = 1{,}000$ Pa.

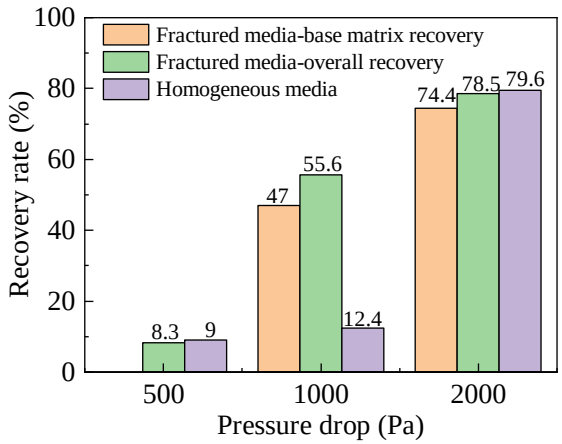

Fig. 9. Comparisons on CO_2 displacing brine efficiency in homogeneous and fractured porous media: $\Delta p = 500$ Pa, $\Delta p = 1{,}000$ Pa, and $\Delta p = 2{,}000$ Pa.

brine-saturated fracture spaces.

To evaluate the effects of pressure drop and the presence of fractures on the performance of CO_2-brine displacement process, comparative simulations were conducted in both the homogeneous and fractured porous media. The displacement efficiency was assessed in terms of the overall recovery of brine as well as the recovery from the base rock matrix. The results under three different pressure drops of 500, 1,000, and 2,000 Pa are shown in Fig. 9.

Under the lowest pressure drop of 500 Pa, the overall recovery of brine was very limited, indicating that the injected gas could not effectively flood either type of porous media. Only a small fraction of gas remained within the core. When the pressure drop was increased to 1,000 Pa, the recovery of brine in homogeneous media remained low at 12.4%. In fractured media, both the overall recovery and the base matrix recovery increased substantially to 47%-55.6%. These results indicated that fracture networks could significantly enhance the displacement efficiency of the injected gas. They provided low-resistance flow paths that facilitated the movement of gas. The base matrix recovery of 47% was lower than the overall recovery of 55.6%, highlighting the contribution of fracture space to the total displacement efficiency.

Under the highest pressure drop of 2,000 Pa, the overall brine recovery increased markedly to 79.6%. The recovery of brine for base matrix also increased substantially to 74.4%. These results demonstrate that higher driving forces improve the displacement performance of the injected gas. However, considering all three pressure drop scenarios, it can be inferred that once the injected gas achieves breakthrough, the presence of fractures does not always further improve brine recovery. In fractured media, the overall recovery of brine was 78.5%, whereas the corresponding value for the base matrix was 74.4%. These values were slightly lower than the value of 79.6% observed in homogeneous media. This comparison indicates that fracture networks provide limited additional improvement of gas displacement efficiency after breakthrough.

3.4 Parametric study on the influence of IFT and wettability

To reveal the effects of IFT and wettability on the characteristics of multiphase displacement in porous media, a series of parametric simulations were conducted. The simulations focused on the displacement of brine by gas in homogeneous rock sample at the pressure drop value of 1,000 Pa. Various IFT values of 15, 29, 45, and 60 mN/m were applied sequentially in the simulation. For wettability, water receding contact angles of 14° (used in previous simulations), 30°, 60°, and 120° were sequentially employed. The variation in the displacement efficiency of brine under different IFT values is shown in Fig. 10(a). An obvious negative correlation between IFT and the displacement efficiency of brine was observed. At the lowest IFT of 15 mN/m, the gas-driven brine recovery reached the value of 79.8%, indicating successful gas breakthrough in the brine-saturated porous media. When the IFT exceeded the value of 29 mN/m, the brine displacement efficiency remained low at 8.8%-12.4%, suggesting that the ap-

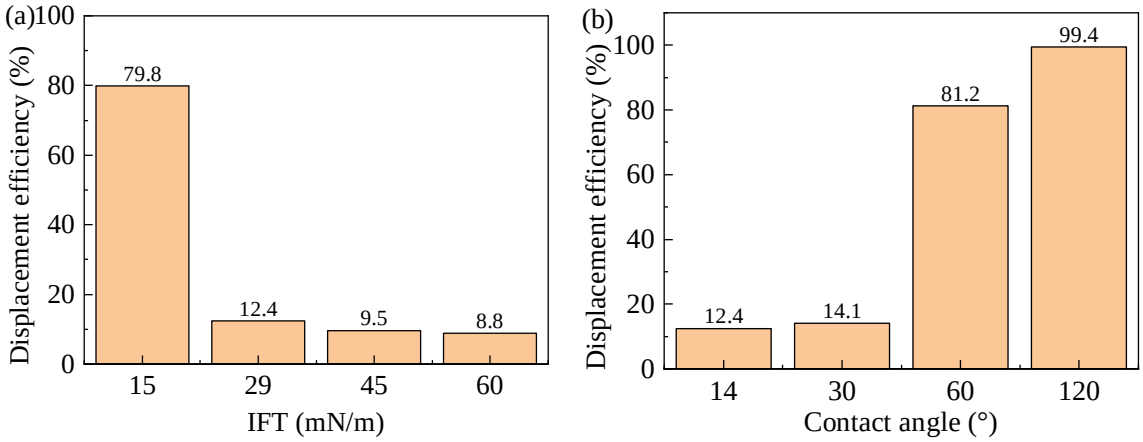

Fig. 10. Parameter study results on (a) IFT and (b) wettability based on CO_2 displacing brine efficiencies in homogeneous porous media under $\Delta p = 1{,}000$ Pa.

plied pressure gradient was insufficient to overcome capillary resistance and sustain effective gas displacement. Furthermore, the effect of wettability on the CO_2-brine displacement process was examined by varying the water-receding contact angle, and the results were shown in Fig. 10(b). Under strongly water-wet conditions, with a contact angle of less than 60°, the brine displacement efficiency remained low at 12.4%-14.1%, indicating that capillary trapping and blockade dominated the flow behaviour. As the wettability shifted to intermediate-wet (60°) and gas-wet (120°), the brine displacement efficiency increased markedly to 81.2%-99.4%. These results demonstrate that altering the wettability can enhance the gas displacement efficiency. They also suggest that modification of wettability may improve the storage performance of saline aquifers for greenhouse gases.

3.5 Discussion

As demonstrated in the preceding sections, fracture structures significantly enhance the CO_2-brine displacement performance in subsurface formations. This improvement occurs because fractures provide preferential flow paths for the injected gas. The continuously distributed fracture apertures effectively reduce flow resistance, thereby facilitating earlier gas breakthroughs under low pressure drop conditions.

In the present study, the critical pressure drop for CO_2 breakthrough in fractured porous media is found to be 500-1,000 Pa. This range is substantially lower than the values of 1,000-2,000 Pa that are observed in homogeneous porous media. This comparison highlights the dominant role of fracture-induced permeability enhancement in lowering the macroscopic displacement threshold. However, the simulation results also indicate that the presence of fractures alone does not guarantee efficient displacement under low driving forces. At a low pressure drop of 500 Pa, evident flow blockade is observed in fractured media, as illustrated in Figs. 6(a) and 7(a). This suggests that capillary trapping remains a limiting mechanism, even with high-permeability fracture channels. This behaviour arises from the combined effects of IFT and rock wettability. These factors govern capillary entry pressures and phase connectivity during multiphase displacement processes (Teng et al., 2022; Zhang et al., 2025). These findings imply that fracture-enhanced flow primarily reduces viscous resistance, however cannot fully overcome capillary barriers under insufficient pressure gradients. Consequently, improving the geological storage efficiency of CO_2 in fractured saline aquifers requires a coupled strategy that simultaneously enhances the viscosity-driven flow and mitigates capillary trapping.

As demonstrated in the parametric analysis, various approaches such as reduction of IFT and modification of the wettability of rock surfaces can effectively reduce capillary resistance. Previous studies have illustrated the crucial effect of reducing IFT and altering wettability on enhancing the multiphase displacement and CO_2 storage efficiency. For example, Lu et al. (2021) suggested that altering shale wettability from water-wet to CO_2-wet can facilitate the underground storage of CO_2. Wan et al. (2022) numerically demonstrated that system wettability and IFT dominated the water-oil displacement efficiency in low-permeability cores. Dong et al. (2025) quantified the positive effects of reducing IFT and altering wettability on the storage performance of H_2 during the displacement and reinjection processes. Similarly, under low IFT conditions, Wang et al. (2025) reported that injected CO_2 could penetrate small-scale porous spaces, reproducing experimental oil recovery results on miscible CO_2 displacement processes. Collectively, these studies provide experimental and numerical evidence supporting the strategies proposed in the current work. More specifically, reducing IFT and modifying wettability can alleviate capillary trapping and improve the displacement efficiency of CO_2 in both fractured and homogeneous porous media.

4. Conclusions

In this study, the displacement of brine using CO_2 is numerically investigated in both the homogeneous and fractured porous media under reservoir conditions of 70 °C and 20 MPa. Digital rock technology was employed to construct the homogeneous and fractured porous media. Moreover,

CFD simulations were performed to resolve the two-phase displacement processes within the complex porous structures. Simulation results of the two-phase fluid distribution inside the porous core samples as well as the brine displacement efficiency are analyzed. The following conclusions are drawn.

1) There exists a critical pressure gradient to achieve gas breakthrough across brine-saturated porous media. For the simulation cases studied in this work, the critical pressure drop for homogeneous porous media lies within the range of 1,000-2,000 Pa. In fractured porous media, the critical pressure drop is reduced by approximately 50% to 500-1,000 Pa. Fracture structures provide low-resistance paths and promote CO_2-brine displacement.
2) Capillary trapping phenomenon is revealed based on two-phase fluid distribution and streamline analyses. Under low pressure drop conditions, fluid blockade occurs predominantly in the smallest pore throats of homogeneous porous media at $\Delta p < 1{,}000$ Pa. In fractured porous media, blockade is mainly observed within fracture structures at $\Delta p < 500$ Pa.
3) A higher pressure gradient is required to overcome capillary blockade and improve the displacement efficiency of brine. In homogeneous porous media, the recovery efficiency of brine reaches 79.6% at the pressure drop of 2,000 Pa, whereas it remains only 12.4% at the pressure drop of 1,000 Pa. In fractured porous media, gas breakthrough does not occur at the pressure drop of 500 Pa. When the pressure drop is increased to a value of 1,000 Pa, the base-matrix displacement efficiency rises to 47%. When the pressure drop is increased to 2,000 Pa, the displacement efficient of base-matrix further increases to 74.4%.
4) Parametric studies reveal that reducing the IFT to 15 mN/m significantly enhances the displacement efficiency of brine. A similar improvement is achieved by altering the wettability from water-wet to gas-wet conditions. Under these favoable conditions, the recovery of brine reaches 79.8%-99.4% for gas-driven displacement in homogeneous porous media. All simulations are conducted at a pressure drop of 1,000 Pa.

Acknowledgements

The paper is finished under the Graduate Tutor Foundation of Qingdao University of Science and Technology (No. 120202190414).

Conflicts of interest

The authors declare no competing interest.

References

Adebayo, A. R. Viability of foam to enhance capillary trapping of CO_2 in saline aquifers–an experimental investigation. International Journal of Greenhouse Gas Control, 2018, 78: 117-124.

Al-Zaidi, E., Fan, X., Edlmann, K. Supercritical CO_2 behaviour during water displacement in a sandstone core sample. International Journal of Greenhouse Gas Control, 2018, 79: 200-211.

ANSYS Inc. ANSYS Fluent User's Guide, Release 2022. ANSYS Inc., 2022.

AP1700 Material Property Query Platform. AP1700 Material Property Query Platform. 2025.

Aslannezhad, M., Tang, D., Bason, D., et al. Digital core analysis and pore network modeling of CO_2 flow and trapping in the Otway Basin. Energy & Fuels, 2025, 39(32): 15369-15385.

Blunt, M. J., Bijeljic, B., Dong, H., et al. Pore-scale imaging and modelling. Advances in Water Resources, 2013, 51: 197-216.

Cao, S., Dai, S., Jung, J. Supercritical CO_2 and brine displacement in geological carbon sequestration: Micromodel and pore network simulation studies. International Journal of Greenhouse Gas Control, 2016, 44: 104-114.

Chang, C., Kneafsey, T. J., Zhou, Q. Experimental study of three-dimensional CO_2-water drainage and fracture-matrix interactions in fractured porous media. Advances in Water Resources, 2021, 155: 104008.

Diao, Z., Li, S., Liu, W., et al. Numerical study of the effect of tortuosity and mixed wettability on spontaneous imbibition in heterogeneous porous media. Capillarity, 2024, 4(3): 50-62.

Ding, B. X., Kantzas, A., Firoozabadi, A. Spatiotemporal X-ray imaging of neat and viscosified CO_2 in displacement of brine-saturated porous media. SPE Journal, 2024, 29(8): 4426-4441.

Dong, Z., Wang, D., Yang, S., et al. Mechanism exploration of the hydrodynamic trapping of hydrogen in geological formations via pore-scale numerical studies. International Journal of Hydrogen Energy, 2025, 159: 150509.

Du, D., Li, Y., Chao, K., et al. Laboratory study of the non-Newtonian behavior of supercritical CO_2 foam flow in a straight tube. Journal of Petroleum Science and Engineering, 2018, 164: 390-399.

Du, D., Zhang, N., Li, Y., et al. Parametric studies on foam displacement behavior in layered heterogeneous porous media based on a stochastic population balance model. Journal of Natural Gas Science and Engineering, 2017, 48: 1-12.

Du, D., Zhang, Z., Song, G., et al. A new prediction model on the effective thermal conductivity of fluid saturated consolidated rock media via the pore-scale numerical study. International Journal of Heat and Mass Transfer, 2026, 260: 128491.

Han, J., Han, S., Kang, D., et al. Application of digital rock physics using X-ray CT for study on alteration of macropore properties by CO_2 EOR in a carbonate oil reservoir. Journal of Petroleum Science and Engineering, 2020, 189: 107009.

Hu, R., Wan, J., Kim, Y., et al. Wettability effects on supercritical CO_2-brine immiscible displacement during drainage: Pore-scale observation and 3D simulation. International

Journal of Greenhouse Gas Control, 2017, 60: 129-139.
Krevor, S. C. M., Pini, R., Zuo, L., et al. Relative permeability and trapping of CO_2 and water in sandstone rocks at reservoir conditions. Water Resources Research, 2012, 48(2): W02532.
Kumari, P., Yahmadi, R., Mumtaz, F., et al. CO_2 capture via subsurface mineralization: Geological settings and engineering perspectives towards long-term storage and decarbonization in the Middle East. Carbon Capture Science and Technology, 2024, 13: 100293.
Li, S., Liang, Y., Jiang, F., et al. Multiscale simulation of water/oil displacement with dissolved CO_2: Implications for geological carbon storage and CO_2-enhanced oil recovery. Chemical Engineering Journal, 2024, 409: 155936.
Liu, J., Yu, P., Li, Y., et al. Numerical simulation on convective heat transfer characteristics in porous media based on digital rock technology. International Journal of Heat and Mass Transfer, 2022, 196: 123323.
Liu, J., Xiao, D., Li, J., et al. Enhanced oil recovery via CO_2 flooding in tight reservoirs: A pore-scale analysis. Advances in Geo-Energy Research, 2025, 17(2): 162-175.
Liu, Z., Cui, P., Cui, X., et al. Prediction of CO_2 solubility in NaCl brine under geological conditions with an improved binary interaction parameter in the Søreide-Whitson model. Geothermics, 2022, 105: 102544.
Li, Y., Wang, X., Yu, P., et al. A pore-scale numerical study on the two-phase flow characteristics in fractured porous media. Colloids and Surfaces A: Physicochemical and Engineering Aspects, 2024, 684: 133257.
Li, Y., Zhao, D., Du, D. Computational study on the three-phase displacement characteristics of foam fluids in porous media. Journal of Petroleum Science and Engineering, 2022, 215: 110732.
Lu, Y., Tian, R., Liu, W., et al. Mechanisms of shale water wettability alteration with chemical groups after CO_2 injection: Implications for shale gas recovery and CO_2 geostorage. Journal of Natural Gas Science and Engineering, 2021, 90: 103922.
Muñoz-Ibáñez, A., Falcon-Suarez, I. H., Marín-Moreno, H., et al. Transport properties of saline CO_2 storage reservoirs with unconnected fractures from brine-CO_2 flow-through tests. Journal of Petroleum Science and Engineering, 2020, 184: 106551.
Najafi, A., Siavashi, J., Ebadi, M., et al. Using computational fluid dynamics to compute the pore-scale CO_2-brine relative permeability. Fuel, 2023, 341: 127715.
Patmonoaji, A., Zhang, Y., Xue, Z., et al. Experimental and numerical simulation of supercritical CO_2 microbubble injection into a brine-saturated porous medium. International Journal of Greenhouse Gas Control, 2019, 91: 102830.
Peng, M., Zhou, Y., Yang, J., et al. Experimental investigation and multi-scale simulations of CO_2 foam flooding for enhanced oil recovery. Capillarity, 2025, 16(2): 39-50.
Ramstad, T. Bentheimer micro-CT with waterflood. Digital Porous Media Portal, 2018.
Ren, X., Sun, L., Yu, H., et al. Study on carbon dioxide flow and storage mechanisms in marine saline aquifers based on digital rock analysis. Geoenergy Science and Engineering, 2025, 246: 213591.
Ryou, J. E., Gang, S., Lee, J. Y., et al. Assessing surfactant influence on CO_2 injection efficiency in geological storage: A pore network approach. Fuel, 2025, 381: 133598.
Saeedi, A., Rezaee, R., Evans, B., et al. Multiphase flow behaviour during CO_2 geo-sequestration: Emphasis on the effect of cyclic CO_2-brine flooding. Journal of Petroleum Science and Engineering, 2011, 79(3-4): 65-85.
Saraji, S., Piri, M., Goual, L. Effects of SO_2 contamination, brine salinity, pressure, and temperature on dynamic contact angles and interfacial tension of supercritical CO_2/brine/quartz systems. International Journal of Greenhouse Gas Control, 2014, 28: 147-155.
Seyyedi, M., Giwelli, A., White, C., et al. Effects of geochemical reactions on multiphase flow in porous media during CO_2 injection. Fuel, 2020, 269: 117421.
Shao, J., Wang, Z., Huang, B., et al. Wetting and injecting effects on CO_2 distribution: Pore-scale micromodel and simulation. Advances in Geo-Energy Research, 2025, 18(2): 99-108.
Song, G., Wang, D., Li, Y., et al. Pore-scale numerical studies on determination of the effective thermal conductivity of fluid-saturated porous media. International Journal of Heat and Mass Transfer, 2025, 238: 126472.
Song, X., Cui, X., Jiang, L., et al. Multi-parameter screening study on static properties of nanoparticle-stabilized CO_2 foam near the CO_2 critical point. Arabian Journal of Chemistry, 2022, 15(3): 103676.
Teng, Y., Wang, P., Xie, H., et al. Capillary trapping characteristics of CO_2 sequestration in fractured carbonate rock and sandstone using MRI. Journal of Natural Gas Science and Engineering, 2022, 108: 104809.
Tronci, G., Buffo, A., Vanni, M., et al. Validation of the diffusion mixture Model for the simulation of bubbly flows and implementation in OpenFOAM. Computers & Fluids, 2021, 227: 105026.
Wan, C., Liu, J., Yu, P., et al. Study of the water displacing oil process in low permeability porous media based on digital rock technology. Colloids and Surfaces A: Physicochemical and Engineering Aspects, 2022, 649: 129469.
Wang, D., Liu, C., Li, Z., et al. Exploration of oil recovery enhancement mechanisms for miscible CO_2 flooding in low-permeability porous media via multiscale pore-scale geometry studies. Chemical Engineering Research and Design, 2025, 224: 181-192.
Wang, H., Cai, J., Su, Y., et al. Pore-scale study on shale oil-CO_2-water miscibility, competitive adsorption, and multiphase flow behaviors. Langmuir, 2023, 39(34): 12226-12234.
Wang, Y., Wang, F., Wang, J., et al. Density-driven convection in layered and stochastically heterogeneous formations: Implications for CO_2 geological sequestratione. Capillarity, 2026, 18(1): 27-40.
Xiao, Y., He, Y., Zheng, J., et al. Modeling of two-phase flow

in heterogeneous wet porous media. Capillarity, 2022, 5(3): 41-50.

Yang, M., Wang, D., Dong, Z., et al. Insight into permeability effects on forced convective heat transfer characteristics in porous media based on pore-scale numerical study. International Communications in Heat and Mass Transfer, 2025, 165: 109004.

Yang, Y., Wang, J., Wang, J., et al. Pore-scale numerical simulation of supercritical CO_2-brine two-phase flow based on the VOF method. Natural Gas Industry B, 2023, 10(5): 466-475.

Zeidan, D., Bähr, P., Farber, P., et al. Numerical investigation of a mixture two-phase flow model in two-dimensional space. Computers & Fluids, 2019, 181: 90-106.

Zhang, Y., Kogure, T., Nishizawa, O., et al. Different flow behavior between 1-to-1 displacement and co-injection of CO_2 and brine in Berea sandstone: Insights from laboratory experiments with X-ray CT imaging. International Journal of Greenhouse Gas Control, 2017, 66: 76-84.

Zhang, Z., Wang, X., Niu, L., et al. Unveiling the roles of sub-resolution pore structures on multiphase fluid flow characteristics in porous media via super-resolution GAN and CFD simulation. Chemical Engineering Research and Design, 2025, 221: 130-144.

Zhao, J., Yao, C., Zhou, C., et al. Pore-scale investigation on dynamic transport characteristics of CO_2 storage in deep saline aquifers. Geoenergy Science and Engineering, 2025, 247: 213703.